Journal of the European Ceramic Society 40 (2020) 4029–4034

Contents lists available at ScienceDirect

Journal of the European Ceramic Society

journal homepage: www.elsevier.com/locate/jeurceramsoc

Original Article

# Direct Integration of Cold Sintered, Temperature-Stable $Bi_2Mo_2O_9$-$K_2MoO_4$ Ceramics on Printed Circuit Boards for Satellite Navigation Antennas

Dawei Wang[a,*,1], Beatia Siame[a,1], Shiyu Zhang[b,1], Ge Wang[a], Xingshen Ju[a], Jinglei Li[c], Zhilun Lu[a], Yiannis Vardaxoglou[b], Will Whittow[b], Darren Cadman[b], Shikuan Sun[a], Di Zhou[c], Kaixin Song[a,d], Ian M. Reaney[a,*]

[a] Department of Materials Science and Engineering, University of Sheffield, Sheffield S1 3JD, UK
[b] Wolfson School of Mechanical, Electrical and Manufacturing Engineering, Loughborough University, Loughborough LE11 3TU, UK
[c] Electronic Materials Research Laboratory, Key Laboratory of the Ministry of Education & International Center for Dielectric Research, School of Electronic Science and Engineering, Xi'an Jiaotong University, Xi'an 710049, Shaanxi, China
[d] College of Electronics Information, Hangzhou Dianzi University, Hangzhou 310018, China

ARTICLE INFO

*Keywords:*
microwave dielectric ceramics
cold sintering process
microstrip patch antennas

ABSTRACT

$Bi_2Mo_2O_9$-$K_2MoO_4$ (BMO-KMO) composite ceramics with > 95% theoretical density were densified by cold sintering at 150 °C. XRD, Raman, back-scattered SEM and EDX spectroscopy indicated that the BMO and KMO phases coexisted in all composites without inter-diffusion and secondary phases. Temperature coefficient of resonant frequency with near-zero value ~ -1 ppm/°C was acheived for BMO-10%KMO with pemittivity ~ 31 and quality factor ~ 3,000 GHz. Cold-sintered composite ceramics were directly pressed/integrated onto a printed circuit board (PCB) using the Cu metallisation as a ground plane for the design and fabrication of a circularly polarized microstrip patch antenna suitable for satellite navigation systems which achieved efficiencies 87% at 1561 MHz (BeiDou) and 88% at 1575 MHz (GPS/Galileo). The low cost, low energy integration of temperature stable, cold sintered ceramics directly onto a PCB represents a step change in substrate fabrication technology for RF devices.

## 1. Introduction

Microwave (MW) ceramics are widely used in modern wireless communication systems as resonators, couplers, filters, substrates and capacitors. [1] However, conventional ceramic sintering technology at > 1000 °C is commonly used to densify ceramics. [2–5] Low-temperature co-fired ceramics (LTCC, 700-900 °C sintering temperature) and ultra-low temperature co-fired ceramics (ULTCC, 400-600 °C sintering temperature) can be co-sintered with low cost electrodes (Ag, Cu and Al, etc.). [6–15] To date, temperature-stable MW ceramics cannot be directly integrated onto polymer-based printed circuit boards (PCBs) in a single deposition step from powder. To revolutionize radio frequency (RF) manufacturing therefore, low loss (high quality factor, $Q \times f \geq 3000$ GHz), temperature-stable (low temperature coefficient of resonant frequency, TCF = +/-3 ppm/°C), medium permittivity ($8 < \varepsilon_r < 40$) are required that densify at < 200 °C and permit printing/pressing directly onto PCBs, reducing the costs and energy used in manufacturing and increasing functionality.

The cold sintering process (CSP) can densify materials and devices at < 200 °C and exhibits great potential for developing novel RF technology and manufacturing processes. Numerous articles have recently appeared on a wide range of materials such as $Li_2MoO_4$ (LMO), $MoO_3$, $Na_2Mo_2O_7$ (NMO), $K_2Mo_2O_7$, $(LiBi)_{0.5}MoO_4$, LMO-PTFE, $Al_2SiO_5$-NaCl, LMO-$Mg_2SiO_4$ and LMO-$BaFe_{12}O_{19}$.[16–31], including a range of temperature stable low loss composites by the present authors, $Na_{0.5}Bi_{0.5}MoO_4$-LMO, $(Bi_{0.95}Li_{0.05})(V_{0.9}Mo_{0.1})O_4$-NMO and $CaTiO_3$-KMO with $8 < \varepsilon_r < 40$.[32–34] Furthermore, standalone RF devices such as temperature stable C0G multilayer ceramic capacitors (MLCCs) and microstrip patch antennas have been fabricated.[34,35] However, the '*holy grail*' of cold-sintered MW ceramics directly pressed/integrated onto PCBs followed by device design and fabrication, has not to date been demonstrated. In this work, $Bi_2Mo_2O_9$ (BMO, $\varepsilon_r$ = 38, TCF = +31 ppm/°C, $Q \times f$ = 12,500) [15,36–38] and KMO ($\varepsilon_r$ = 6.4, TCF = -70 ppm/°C, $Q \times f$ = 26,500)[33,34] were selected with the intent of fabricating MW composite ceramics with near-zero TCF. Direct integration of these ceramics onto PCBs is demonstrated followed by the

* Corresponding author.
*E-mail addresses:* dawei.wang@sheffield.ac.uk (D. Wang), i.m.reaney@sheffield.ac.uk (I.M. Reaney).
[1] Contributed equally to this work.

https://doi.org/10.1016/j.jeurceramsoc.2020.04.025
Received 28 February 2020; Received in revised form 15 April 2020; Accepted 16 April 2020
Available online 21 April 2020
0955-2219/ © 2020 Elsevier Ltd. All rights reserved.

**Table 1**
Sintering temperature (ST), relative density ($\rho_r$), and MV dielectric properties of BMO-KMO ceramics.

| Composition | ST (°C) | $\rho_r$ (%) | $\varepsilon_r$ | $tan\delta$ | $Q \times f$ (GHz) | TCF (ppm/°C) |
|---|---|---|---|---|---|---|
| BMO | 680 | 95 ± 1.8 | 38 | 0.0004 | 11000 | +31 |
| BMO-5%KMO | 150 | 87.3 ± 2.3 | 28 | 0.001 | 4700 | +17 |
| BMO-10%KMO | 150 | 99.6 ± 1.9 | 31 | 0.002 | 3000 | −1 |
| BMO-20%KMO | 150 | 100 ± 0.6 | 27 | 0.004 | 1600 | −31 |
| BMO-50%KMO | 150 | 100 ± 1.1 | 22 | 0.006 | 1300 | −55 |
| KMO | 150 | 100 ± 1.5 | 6.4 | 0.0003 | 26500 | −70 |

simulation and fabrication of a microstrip patch antenna suitable for satellite navigation systems.

## 2. Experimental

(1-x)BMO-xKMO (x = 5 wt%, 10 wt%, 20 wt%, 50 wt%, 100 wt%) composite ceramics were prepared by CSP. BMO powder was synthesised by the solid-state reaction method. Raw chemicals $Bi_2O_3$ (99.9%, Acros Organics) and $MoO_3$ (> 99%, Acros Organics) were weighed with a $Bi_2O_3$: $MoO_3$ ratio of 1:2 and ball-milled 4 h in solvent isopropanol. The mixed powders were dried, calcined 4 h at 630-650 °C to synthesize the compound and ball-milled 4 h in isopropanol to reduce particle size. [15,36–38] KMO (Alfa Aesar, > 95%) and BMO powders were mixed with 5-10 wt% deionized water, hot-pressed 30 min at 150 °C and 600 MPa (Atlas Heated Platens, Specac) and dried 24 h at 120 °C to remove residual moisture. BMO ceramics were conventionally sintered at 680 °C for 2 h.

The densities of ceramic samples were measured by a geometric method.[17–34] Crystal structure, phase assemblage and microstructure were determined by Bruker D2 Phaser X-ray powder diffraction (XRD, Cu$K\alpha$ radiation), Renishaw inVia Raman microscope Raman spectroscopy and FEI Inspect F-50 scanning electron microscopy (SEM). The $TE_{01\delta}$ mode was employed to measure the MV dielectric properties of ceramics using an Advantest R3767CH vector network analyzer. The cavity was heated by a Peltier device and the resonant frequency ($f$) was measured from 25 °C to 85 °C. The corresponding TCF values were obtained using the formula:

$$TCF = \frac{f_T - f_{T_0}}{f_{T_0} \times (T - T_0)} \times 10^6 \quad (1)$$

where the $f_T$ and $f_{T_0}$ are the $TE_{01\delta}$ resonant frequencies at temperatures, T and $T_0$, respectively.

## 3. Results and discussion

The relative density ($\rho_r$) of cold-sintered BMO-xKMO composites increases from 90% for BMO-5%KMO to 100% for x > 0.05, Table 1, confirming that dense BMO-xKMO composites are readily fabricated by cold sintering.

The XRD patterns of cold-sintered BMO-xKMO ceramics are given in Fig. 1(a). Both BMO and KMO are monoclinic with *P121/n1* (ICSD: 201742) and *C12/m1* (ICSD: 16154) symmetry, respectively. [15,33,34,36–38] B-site $Mo^{6+}$ cations are coordinated by four O-anions, leading to tightly bound $MoO_4$ tetrahedra. The A-site $Bi^{3+}$ or $K^+$ cations are circled by eight or six O anions, as displayed in the schematic crystal structures of BMO and KMO (Fig. 1c). Diffraction peaks in the XRD patterns of BMO-xKMO composites may all be ascribed to either BMO and KMO. The diffraction peak intensity of KMO increases with the weight fraction of KMO increasing, as marked in Fig. 1(a) but no impurity peaks, nor shift in peak position are observed.

To further evaluate the phase composition and lattice parameters of BMO-KMO, full-pattern Rietveld refinement of BMO-10%LMO was performed using a Topas 5 software, where a two-phase refinement (*C12/m1* + *P121/n1*) is used. Low values of *GOF* = 1.65, $R_{exp}$ = 7.2% and $R_{wp}$ = 11.8% indicate that the calculated result agrees with the observed pattern, Fig. 1(b). The weight fraction of BMO (*C12/m1*, 89%) and KMO (*P121/n1*, 11%) phases is determined for BMO-10%KMO, close to the nominal composition. The calculated lattice parameters are $a$ = 11.9515 Å, $b$ = 10.8007 Å, $c$ = 11.8814 Å for BMO and $a$ = 12.672 Å, $b$ = 6.030 Å, $c$ = 7.066 Å for KMO, respectively, which agree with the reported values. [15,33,34,36–38]

The room-temperature Raman data of BMO-xKMO composites is

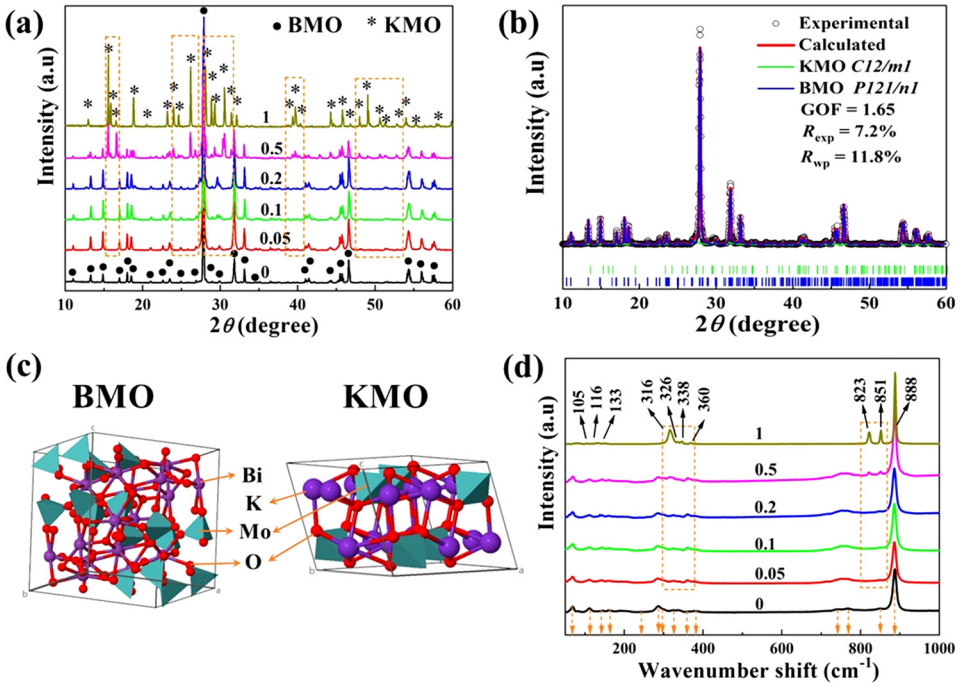


**Fig. 1.** (a) XRD patterns of BMO-xKMO ceramic composites. (b) Rietveld refinement of BMO-10%KMO. The schematic crystal structures of (c) BMO and KMO. (d) Raman spectra of BMO-xKMO ceramic composites.

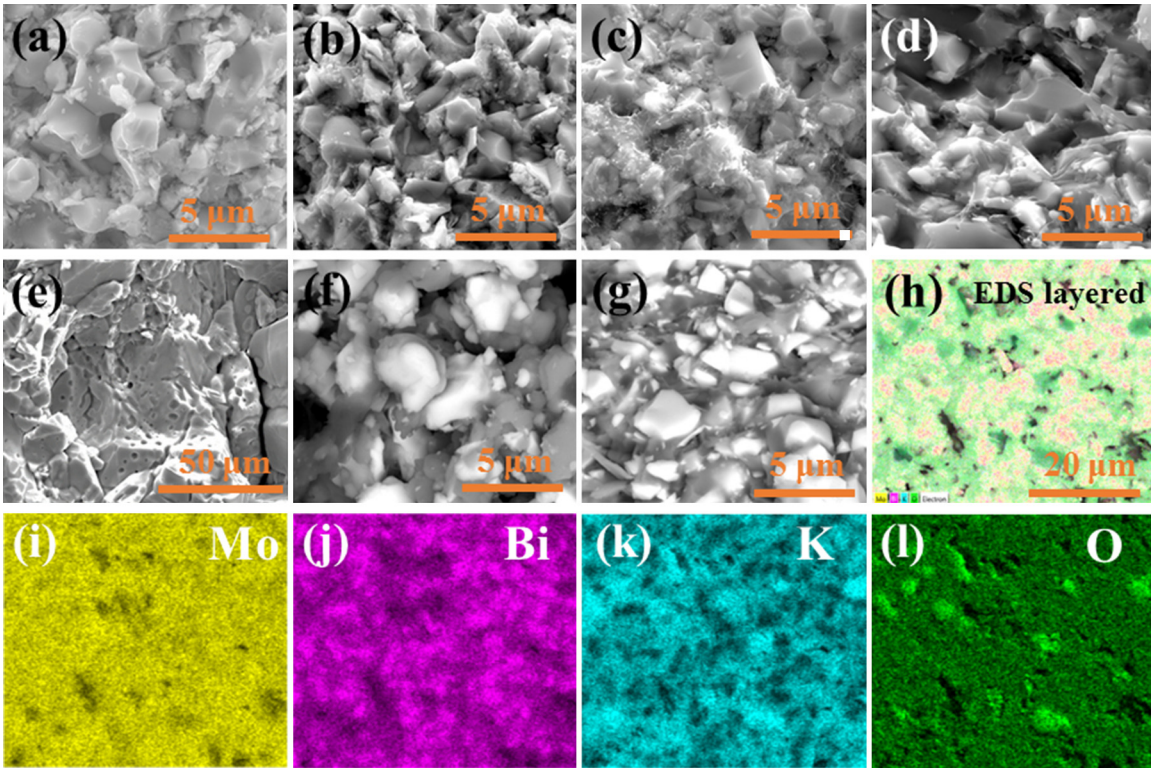


**Fig. 2.** SEM images of the cross-section for cold-sintered BMO-xKMO (a) 5%, (b) 10%, (c) 20%, (d) 50%, (e) 100%. BSE images of (f) mixed BMO and KMO powder, (g) cold-sintered BMO-50%KMO cross-section. EDS mapping images of cold-sintered BMO-50%KMO samples: (h) elemental layered image, (i) Mo, (j) Bi, (k) K, (l) O.

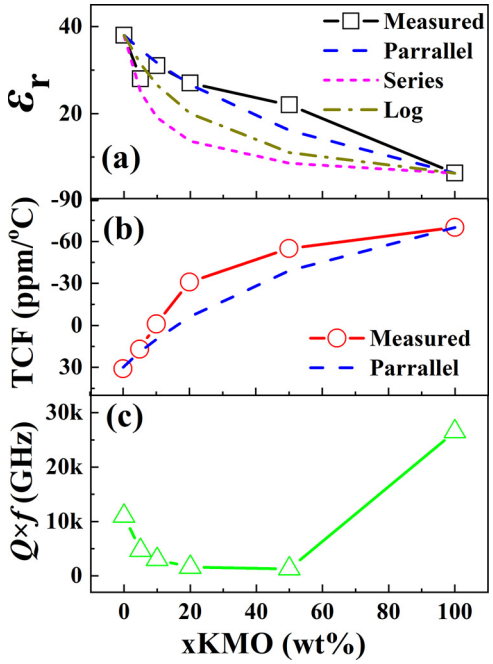


**Fig. 3.** Microwave properties of BMO-xKMO composites *vs.* KMO weight fraction.

shown in Fig. 1(d). In agreement with previous reports, [39,40] 14 Raman bands are observed in the spectrum of BMO at 68, 114, 142, 176, 260, 284, 296, 321, 358, 380, 739, 768, 851 and 888 $cm^{-1}$, which were assigned to bending (260 ~ 380 $cm^{-1}$) and stretching (739 ~ 888 $cm^{-1}$) modes of $MoO_4$ tetrahedra and the conversion of Mo/Bi atoms (< 260 $cm^{-1}$), respectively. According to group theory, there are 39 different vibrational modes in KMO[41,42]:

$$\Gamma_{KMO} = 13A_g + 7A_u + 8B_g + 11B_u \quad (3)$$

The Raman bands in the range of 100 ~ 160 $cm^{-1}$ correspond to a combination of the translations and vibrations of $MoO_4$ tetrahedra and translations of K ions. The 310 ~ 370 $cm^{-1}$ bands are related to bending modes of $MoO_4$ tetrahedra. The 820 ~ 890 $cm^{-1}$ bands are related to stretching modes of $MoO_4$ tetrahedra. Raman spectra of BMO-KMO composites therefore, constitute an overlay of Raman bands from individual phases (Fig. 1d). The intensity of Raman modes for KMO increases gradually with increase in x.

SEM images of the cross-section for the cold-sintered BMO-KMO samples are given in Fig. 2(a–e). All compositions with x > 0.05 have dense microstructures, in agreement with measured densities in Table 1. The dark and light regions of contrast in BSE images of mixed BMO-KMO powder (Fig. 2f) and cold-sintered BMO-50%KMO (Fig. 2g) suggest that two chemically distinct KMO and BMO rich phases are present which is confirmed by EDS mapping (Fig. 2h–l) and in agreement with Raman spectra and XRD patterns (Fig. 1).

Fig. 3 shows the MV dielectric properties of BMO-xKMO ceramic composites with increase of KMO weight fraction, Table 1. $\varepsilon_r$ and TCF linearly decrease from 39 and +31 ppm/°C, to 6.4 and -70 ppm/°C, respectively. $Q \times f$ of BMO-xKMO composites ceramics is lower than both end members and in the range of 1300 ~ 4700, likely due to residual amorphous phase in cold-sintered systems.[16–34] Near-zero value of TCF (-1 ppm/°C) is obtained for BMO-10%KMO with $\varepsilon_r$ ~ 31 and $Q \times f$ ~ 3,000 GHz. The effective $\varepsilon_r$ can be calculated by the following mixing laws:[32–34]

$$\text{parallel law, } \varepsilon = V_1 \varepsilon_1 + V_2 \varepsilon_2 \quad (4)$$

$$\text{series law, } 1/\varepsilon = V_1/\varepsilon_1 + V_2/\varepsilon_2 \quad (5)$$

$$\text{logarithmic law, } \varepsilon = \varepsilon_1^{V_1}\varepsilon_2^{V_2} \text{ i. e. } \lg\varepsilon = V1\lg\varepsilon 1 + V2\lg\varepsilon 2 \quad (6)$$

where $\varepsilon_1$ is the $\varepsilon_r$ of phase 1, $\varepsilon_2$ is the $\varepsilon_r$ of phase 2, $V_1$ is the volume fraction of phase 1 and $V_2$ (1- $V_1$ = $V_2$) is the volume fraction of phase 2. $\varepsilon_r$ follows a parallel mixing law, Fig. 3(a), which may also be used to

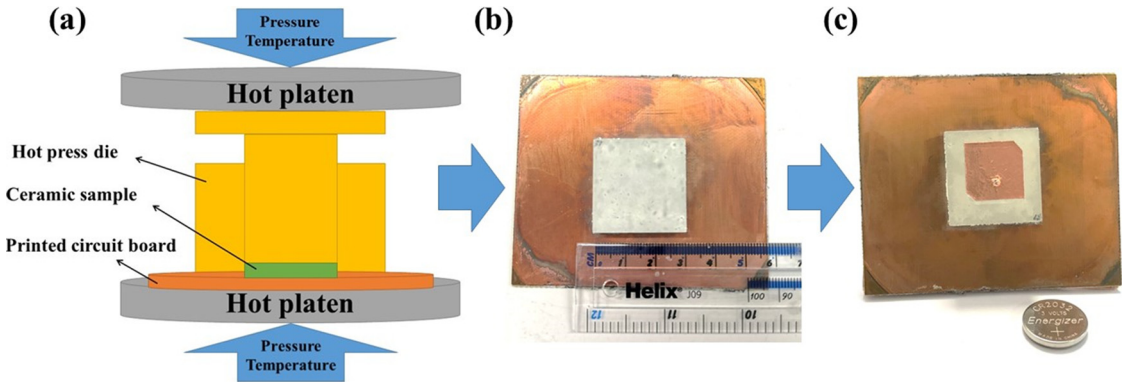


**Fig. 4.** (a) The schematic diagram of cold-sintering ceramic substrate for antenna. (b) cold-sintered BMO-10%KMO ceramic substrate with a dimension of 30 mm × 30 mm × 7 mm on an 85 mm × 75 mm × 1.6 mm glass-reinforced epoxy laminate PCB (FR4). (c) The fabricated antenna with cold-sintered BMO-10% KMO ceramic as substrate.

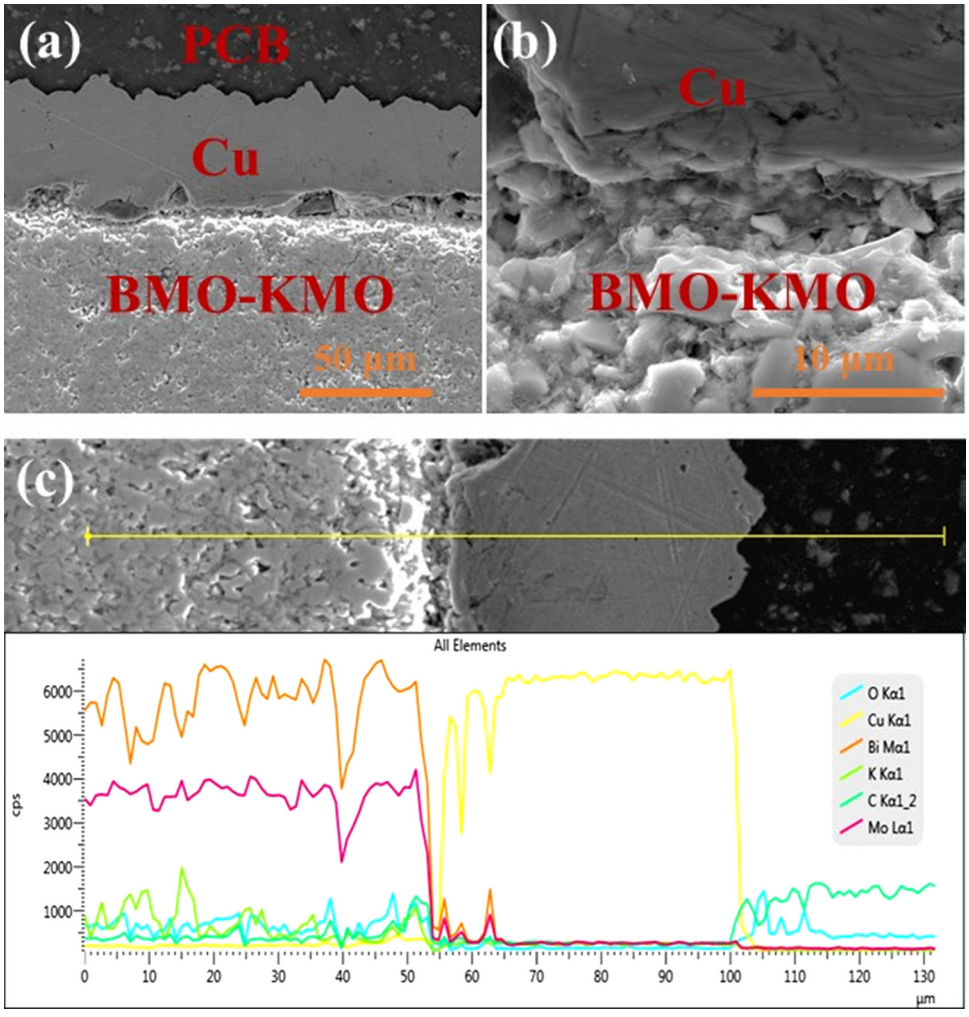


**Fig. 5.** (a, b) SEM images (c) EDS elemental line-scans of a cross-section of cold-sintered BMO-10%KMO on a Cu metallised PCB.

predict TCF, according to:

$$TCF = V_1TCF_1 + V_2TCF_2 \quad (7)$$

where $TCF_1$ and $TCF_2$ are the temperature coefficients of phase 1 and 2, respectively, Fig. 3(b).

Satellite navigation systems are widely used in consumer electronics and provide navigation, localization, and tracking. The Global Satellite Navigation System (GLONAS), Global Positioning System (GPS), Gallileo and Beidou were installed by Russia, United states, Europe and China, respectively and all operate around 1.5-1.6 GHz. The antenna is one of the key components to ensure low latency, good reception to provide high precision positioning and robust communication. Microstrip patch antennas are a popular choice in modern electronics due to their low-profile, low-cost, ease of fabrication and their small physical size for integration into limited space. Generally, ceramic dielectrics with overall dimensions of 20 mm × 20 mm × 2 mm to 40 mm × 40 mm × 7 mm have been widely used as the substrates for

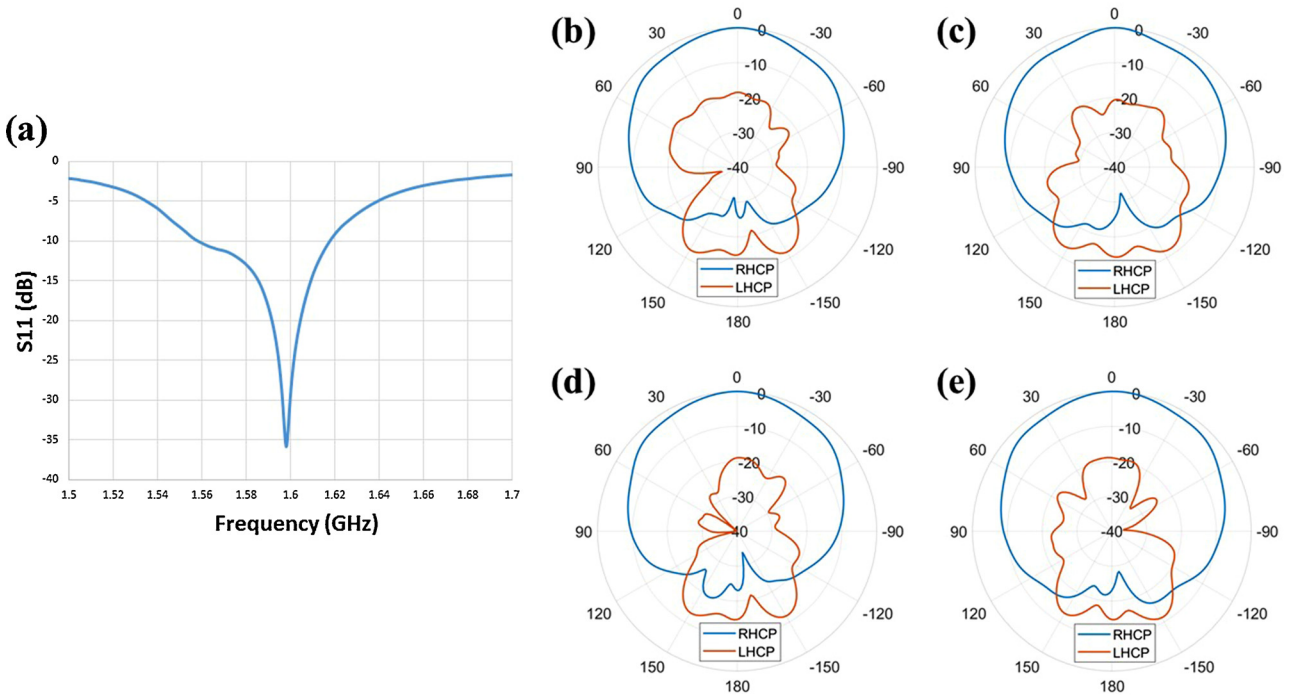


**Fig. 6.** (a) Measured S11 curve; Measured radiation patterns in Azimuth (b) and Elevation plane (c) at 1561 MHz; Measured radiation patterns in Azimuth (d) and Elevation plane (e) at 1575 MHz.

**Table 2**
Measured antenna performance of the fabricated ceramic microstrip patch antenna at two frequency bands.

| Parameters | BeiDou | GPS/Galileo |
|---|---|---|
| Frequency | 1561 MHz | 1575 MHz |
| Polarization | RHCP | RHCP |
| Gain | 5.7 dBic | 5.8 dBic |
| Directivity | 6.4 dBic | 6.4 dBic |
| Total efficiency | 87% | 88% |
| Axial ratio | 2.1 dB | 1.9 dB |

satellite navigation antennas for vehicles. Satellite navigation antennas are mainly sold as individual units in which the ceramic is sintered at > 1200 °C and which require assembling using a 'pick and place' procedure. The modular design helps end-users to reduce cost with respect to customization but some highly integrated, direct compact packaged systems require satellite navigation antennas that can be directly fabricated on PCBs. This is impossible with conventionally sintered ceramics (> 1200 °C) but cold sintering densifies powders at less than the melting point (< 200 °C) of the PCB board and hence can be directly pressed onto its surface and fully integrated from a manufacturing perspective.

In this work, BMO-10%KMO ceramic substrates 30 mm × 30 mm × 7 mm were directly cold-sintered onto an 85 mm × 75 mm × 1.6 mm glass-reinforced epoxy laminate PCB (FR4), as schematically indicated in Fig. 4(a). The Cu layer of the FR4 was intentionally not removed and acted as the ground plane (Fig. 4b). For proof of concept, the top patch was cut from a conductive copper tape with dimensions of 18.5 mm × 18.5 mm and two cut corners to achieve circular polarization but for mass production, it could be screen printed using a low temperature binder-burn out conductive ink. The fabricated antenna is shown in Fig. 4(c). The SEM images and EDS elemental line scans of a cross-section of cold-sintered BMO-10%KMO on PCBs are shown in Fig. 5. A Cu layer of ~ 45 μm thick is shown in the enlarged BSE image, Fig. 5(a,c), which has a sharp interface with the ceramic grains, indicating chemical/temperature compatibility with the BMO-KMO layer, further confirmed from the EDS elemental line-scans, Fig. 5(c).

The antenna gave a right-hand circular polarization (RHCP) across a wide operating frequency and supported the B1I (1561 MHz) band for BeiDou, L1 (1575 MHz) GPS and E1 (1575 MHz) for Galileo. The measured S11 is shown in Fig. 6(a), indicating that the ceramic microstrip patch antenna is well matched and has -10 dB bandwidth of 59 MHz that covers the desired frequency 1561 MHz and 1575 MHz. The far-field performance of the antenna was measured in an anechoic chamber and the parameters are summarized in Table 2. The total antenna efficiencies (include the S11 mismatch) are 87% at 1561 MHz (BeiDou) and 88% at 1575 MHz (GPS/Galileo). The axial ratio was < 3 dB at both frequencies which indicated good circular polarization. The circular polarization performance is particularly important for satellite navigation applications since the relative orientation of the transmitting and receiving antennas is not fixed, and the circularly polarization is able to overcome the Faraday rotation effect due to the ionosphere thereby maximising signal reception. The measured radiation patterns at 1561 MHz and 1575 MHz of the ceramic microstrip antenna are shown in Fig. 6(b–e), respectively.

## 4. Conclusions

BMO-KMO microwave ceramic composites with high relative densities (90%-100%) were successfully fabricated by cold sintering at 150 °C/30 min/600 MPa. Only BMO and KMO were presented in composites and no chemical reaction occurred between the two end-members, as confirmed by XRD, Raman, BSE and EDS mapping. With increasing weight fraction of KMO, $\varepsilon_r$ and TCF decreased while $Q \times f$ increased. TCF ~ +1 ppm/°C was achvieved in BMO-10%KMO with $Qf$ ~ 3,000 GHz and $\varepsilon_r$ ~ 31. An antenna for satellite navigation was designed and then fabricated using a BMO-10%KMO substrate (30 × 30 × 7 mm) directly pressed onto a PCB metallised circuit board using the Cu layer as a ground plane. The antenna had an S11 of -10 dB with bandwidth of 59 MHz, < 3 dB axial ratio that covers the desired frequency bands 1561 MHz and 1575 MHz. The antenna works well at both BeiDou and GPS/Galileo frequencies with efficiencies of 87% at

1561 MHz and 88% at 1575 MHz.

## Declaration of Competing Interest

The authors declare that they have no known competing financial interests or personal relationships that could have appeared to influence the work reported in this paper.

## Acknowledgments

We thank the funding and supporting from EPSRC (SUbST: EP/L017563/1, SYMETA: EP/N010493/1).

## References

[1] I.M. Reaney, D. Iddles, Microwave dielectric ceramics for resonators and filters in mobile phone networks, J Am Ceram Soc 89 (7) (2006) 2063–2072.
[2] T. Ibn-Mohammed, C.A. Randall, K. Mustapha, J. Guo, J. Walker, S. Berbano, S. Koh, D. Wang, D. Sinclair, I. Reaney, Decarbonising ceramic manufacturing: A techno-economic analysis of energy efficient sintering technologies in the functional materials sector, J Eur Ceram Soc 39 (16) (2019) 5213–5235.
[3] Z. Song, K. Song, B. Liu, P. Zheng, H. Barzegar Bafrooei, W. Su, H. Lin, F. Shi, D. Wang, I. Reaney, Temperature-dependent dielectric and Raman spectra and microwave dielectric properties of gehlenite-type Ca2Al2SiO$_7$ ceramics, International Journal of Applied Ceramic Technology 17 (2) (2020) 771–777.
[4] Q. Lin, K. Song, B. Liu, H.B. Bafrooei, D. Zhou, W. Su, F. Shi, D. Wang, H. Lin, I.M. Reaney, Vibrational spectroscopy and microwave dielectric properties of AY$_2$Si$_3$O$_{10}$ (A= Sr, Ba) ceramics for 5G applications, Ceram Int 46 (1) (2020) 1171–1177.
[5] D. Zhou, D. Guo, W.B. Li, L.X. Pang, X. Yao, D.W. Wang, I.M. Reaney, Novel temperature stable high-$\varepsilon_r$ microwave dielectrics in the Bi$_2$O$_3$–TiO$_2$–V$_2$O$_5$ system, J Mater Chem C 4 (23) (2016) 5357–5362.
[6] H.H. Guo, D. Zhou, W.F. Liu, L.X. Pang, D.W. Wang, J.Z. Su, Z.M. Qi, Microwave dielectric properties of temperature-stable zircon-type (Bi,Ce)VO$_4$ solid solution ceramics, J Am Ceram Soc 103 (1) (2020) 423–431.
[7] H.H. Guo, D. Zhou, L.X. Pang, Z.M. Qi, Microwave dielectric properties of low firing temperature stable scheelite structured (Ca,Bi)(Mo,V)O$_4$ solid solution ceramics for LTCC applications, J Eur Ceram Soc 39 (7) (2019) 2365–2373.
[8] D. Zhou, L.X. Pang, D.W. Wang, I.M. Reaney, BiVO$_4$ based high k microwave dielectric materials: a review, J Mater Chem C 6 (35) (2018) 9290–9313.
[9] D. Zhou, L.X. Pang, D.W. Wang, Z.M. Qi, I.M. Reaney, High quality factor, ultralow sintering temperature Li6B$_4$O$_9$ microwave dielectric ceramics with ultralow density for antenna substrates, Acs Sustain Chem Eng 6 (8) (2018) 11138–11143.
[10] L.X. Pang, D. Zhou, D.W. Wang, J.X. Zhao, W.G. Liu, Z.X. Yue, I.M. Reaney, Temperature stable K0. 5(Nd$_{1-x}$Bi$_x$)0.5MoO$_4$ microwave dielectrics ceramics with ultra-low sintering temperature, J Am Ceram Soc 101 (5) (2018) 1806–1810.
[11] D. Zhou, L.X. Pang, D.W. Wang, H.H. Guo, F. Yang, Z.M. Qi, C. Li, B.B. Jin, I.M. Reaney, Crystal structure, impedance and broadband dielectric spectra of ordered scheelite-structured Bi(Sc$_{1/3}$Mo$_{2/3}$)O$_4$ ceramic, J Eur Ceram Soc 38 (4) (2018) 1556–1561.
[12] D. Zhou, L.X. Pang, D.W. Wang, C. Li, B.B. Jin, I.M. Reaney, High permittivity and low loss microwave dielectrics suitable for 5G resonators and low temperature co-fired ceramic architecture, J Mater Chem C 5 (38) (2017) 10094–10098.
[13] D. Zhou, J. Li, L.-X. Pang, D.-W. Wang, I.M. Reaney, Novel water insoluble (Na$_x$Ag$_{2-x}$) MoO$_4$ ($0 \leq x \leq 2$) microwave dielectric ceramics with spinel structure sintered at 410 degrees, J Mater Chem C 5 (24) (2017) 6086–6091.
[14] D. Zhou, J. Li, L.-X. Pang, G.-H. Chen, Z.-M. Qi, D.-W. Wang, I.M. Reaney, Crystal structure, infrared spectra, and microwave dielectric properties of temperature-stable zircon-type (Y,Bi)VO$_4$ solid-solution ceramics, Acs Omega 1 (5) (2016) 963–970.
[15] R. Gheisari, H. Chamberlain, G. Chi-Tangyie, S. Zhang, A. Goulas, C.-K. Lee, T. Whittaker, D. Wang, A. Ketharam, A. Ghosh, Multi-material additive manufacturing of low sintering temperature Bi2Mo2O$_9$ ceramics with Ag floating electrodes by selective laser burnout, Virtual and Physical Prototyping 15 (2) (2020) 133–147.
[16] H. Kahari, M. Teirikangas, J. Juuti, H. Jantunen, Dielectric Properties of Lithium Molybdate Ceramic Fabricated at Room Temperature, J Am Ceram Soc 97 (11) (2014) 3378–3379.
[17] H. Kahari, M. Teirikangas, J. Juuti, H. Jantunen, Room-temperature fabrication of microwave dielectric Li$_2$MoO$_4$-TiO$_2$ composite ceramics, Ceram Int 42 (9) (2016) 11442–11446.
[18] M. Vaataja, H. Kahari, J. Juuti, H. Jantunen, Li$_2$MoO$_4$-based composite ceramics fabricated from temperature- and atmosphere-sensitive MnZn ferrite at room temperature, J Am Ceram Soc 100 (8) (2017) 3626–3635.
[19] M. Vaataja, H. Kahari, K. Ohenoja, M. Sobocinski, J. Juuti, H. Jantunen, 3D printed dielectric ceramic without a sintering stage, Sci Rep-Uk 8 (2018).
[20] J. Guo, H.Z. Guo, A.L. Baker, M.T. Lanagan, E.R. Kupp, G.L. Messing, C.A. Randall, Cold Sintering: A Paradigm Shift for Processing and Integration of Ceramics, Angew Chem Int Edit 55 (38) (2016) 11457–11461.
[21] J. Guo, S.S. Berbano, H.Z. Guo, A.L. Baker, M.T. Lanagan, C.A. Randall, Cold Sintering Process of Composites: Bridging the Processing Temperature Gap of Ceramic and Polymer Materials, Adv Funct Mater 26 (39) (2016) 7115–7121.
[22] A. Baker, H.Z. Guo, J. Guo, C. Randall, Utilizing the Cold Sintering Process for Flexible-Printable Electroceramic Device Fabrication, J Am Ceram Soc 99 (10) (2016) 3202–3204.
[23] J. Guo, A.L. Baker, H.Z. Guo, M. Lanagan, C.A. Randall, Cold sintering process: A new era for ceramic packaging and microwave device development, J Am Ceram Soc 100 (2) (2017) 669–677.
[24] J.P. Maria, X.Y. Kang, R.D. Floyd, E.C. Dickey, H.Z. Guo, J. Guo, A. Baker, S. Funihashi, C.A. Randall, Cold sintering: Current status and prospects, J Mater Res 32 (17) (2017) 3205–3218.
[25] J. Guo, X.T. Zhao, T.H. De Beauvoir, J.H. Seo, S.S. Berbano, A.L. Baker, C. Azina, C.A. Randall, Recent Progress in Applications of the Cold Sintering Process for Ceramic-Polymer Composites, Adv Funct Mater 28 (39) (2018).
[26] I.J. Induja, M.T. Sebastian, Microwave dielectric properties of mineral sillimanite obtained by conventional and cold sintering process, J Eur Ceram Soc 37 (5) (2017) 2143–2147.
[27] W.B. Hong, L. Li, M. Cao, X.M. Chen, Plastic deformation and effects of water in room-temperature cold sintering of NaCl microwave dielectric ceramics, J Am Ceram Soc 101 (9) (2018) 4038–4043.
[28] Y. Liu, P. Liu, C.X. Hu, Low-temperature preparation and microwave dielectric properties of cold sintered Li$_2$Mg$_3$TiO$_6$ nanocrystalline ceramics, Ceram Int 44 (17) (2018) 21047–21052.
[29] S.S. Faouri, A. Mostaed, J.S. Dean, D.W. Wang, D.C. Sinclair, S.Y. Zhang, W.G. Whittow, Y. Vardaxoglou, I.M. Reaney, High quality factor cold sintered Li$_2$MoO$_4$-BaFe$_{12}$O$_{19}$ composites for microwave applications, Acta Mater 166 (2019) 202–207.
[30] D. Zhou, L.X. Pang, D.W. Wang, I.M. Reaney, Novel water-assisting low firing MoO$_3$ microwave dielectric ceramics, J Eur Ceram Soc 39 (7) (2019) 2374–2378.
[31] Y. Ji, K. Song, X. Luo, B. Liu, H. Barzegar Bafrooei, D. Wang, Microwave dielectric properties of (1-x) Li$_2$MoO$_4$-xMg$_2$SiO$_4$ composite ceramics fabricated by cold sintering process, Frontiers in Materials 6 (2019) 256.
[32] D.W. Wang, D. Zhou, S.Y. Zhang, Y. Vardaxoglou, W.G. Whittow, D. Cadman, I.M. Reaney, Cold-Sintered Temperature Stable Na$_{0.5}$Bi$_{0.5}$MoO$_4$-Li$_2$MoO$_4$ Microwave Composite Ceramics, Acs Sustain Chem Eng 6 (2) (2018) 2438–2444.
[33] D.W. Wang, S.Y. Zhang, D. Zhou, K.X. Song, A. Feteira, Y. Vardaxoglou, W. Whittow, D. Cadman, I.M. Reaney, Temperature Stable Cold Sintered (Bi$_{0.95}$Li$_{0.05}$)(V$_{0.9}$Mo$_{0.1}$)O$_4$-Na$_2$Mo$_2$O$_7$ Microwave Dielectric Composites, Materials 12 (9) (2019).
[34] D. Wang, S. Zhang, G. Wang, Y. Vardaxoglou, W. Whittow, D. Cadman, D. Zhou, K. Song, I.M. Reaney, Cold sintered CaTiO$_3$-K$_2$MoO$_4$ microwave dielectric ceramics for integrated microstrip patch antennas, Applied Materials Today 18 (2020) 100519.
[35] D.W. Wang, D. Zhou, K.X. Song, A. Feteira, C.A. Randall, I.M. Reaney, Cold-Sintered C0G Multilayer Ceramic Capacitors, Adv Electron Mater 5 (7) (2019).
[36] D. Zhou, H. Wang, L.X. Pang, C.A. Randall, X. Yao, Bi$_2$O$_3$-MoO$_3$ Binary System: An Alternative Ultralow Sintering Temperature Microwave Dielectric, J Am Ceram Soc 92 (10) (2009) 2242–2246.
[37] D. Zhou, H. Wang, X. Yao, L.X. Pang, Microwave Dielectric Properties of Low Temperature Firing Bi$_2$Mo$_2$O$_9$ Ceramic, J Am Ceram Soc 91 (10) (2008) 3419–3422.
[38] D. Zhou, C.A. Randall, A. Baker, H. Wang, L.X. Pang, X. Yao, Dielectric Properties of an Ultra-Low-Temperature Cofiring Bi$_2$Mo$_2$O$_9$ Multilayer, J Am Ceram Soc 93 (5) (2010) 1443–1446.
[39] F.D. Hardcastle, I.E. Wachs, Molecular-Structure of Molybdenum Oxide in Bismuth Molybdates by Raman-Spectroscopy, J Phys Chem-Us 95 (26) (1991) 10763–10772.
[40] K. Seevakan, A. Manikandan, P. Devendran, Y. Slimani, A. Baykal, T. Alagesan, Structural, magnetic and electrochemical characterizations of Bi$_2$Mo$_2$O$_9$ nanoparticle for supercapacitor application, J Magn Magn Mater 486 (2019).
[41] W. Paraguassu, G.D. Saraiva, S. Guerini, P.T.C. Freire, B.T.O. Abagaro, J. Mendes, Pressure-induced phase transition on K$_2$MoO$_4$: A Raman scattering study and ab initio calculations, J Solid State Chem 196 (2012) 197–202.
[42] G.D. Saraiva, W. Paraguassu, P.T.C. Freire, M. Maczka, J. Mendes, Temperature-dependent Raman scattering study of K$_2$MoO$_4$, Vib Spectrosc 58 (2012) 87–94.